User Shadowing Suppression for 5G mm-wave Mobile Terminal Antennas

Syrytsin, Igor A.; Zhang, Shuai; Pedersen, Gert Frølund; Morris , Arthur S.

Published in:
I E E E Transactions on Antennas and Propagation

DOI (link to publication from Publisher):
10.1109/TAP.2019.2905685

Publication date:
2019

Document Version
Accepted author manuscript, peer reviewed version

This article has been accepted for publication in a future issue of this journal, but has not been fully edited. Content may change prior to final publication. Citation information: DOI 10.1109/TAP.2019.2905685, IEEE Transactions on Antennas and Propagation

User Shadowing Suppression for 5G mm-wave Mobile Terminal Antennas

Igor Syrytsin, Shuai Zhang, *Senior Member IEEE*, Gert Frølund Pedersen, *Senior Member IEEE*, and Art Morris, *Fellow, IEEE*

***Abstract*—In 5G mm-wave mobile terminal applications, the user's body has a very high chance of creating blockage or shadow in the radiation patterns of handset antenna arrays. In this paper, we find that the corner positions of a handset chassis yield the best performance for the 5G mm-wave array system in terms of spatial coverage when user effects are considered. To prove that claim, a prototype of a 5G mm-wave antenna system was constructed using the SIW lens and MMPX connectors and was compared to the more general case. The lens is simulated and measured with the user in talk, data and dual-hand modes. It has been shown that the method proposed in this paper can be used as general guideline for the 5G phased array construction. Finally, two configurations of sub-arrays placed diagonally on the opposite corners of the mobile device were investigated to compare them to each other and to the setup with sub-arrays in all the corners.**

***Index Terms*—Mobile terminal antenna, antenna array, 5G, cm-wave, diversity, user impact.**

I. Introduction

LATELY the topic of beamforming at a mobile terminal for the 5th generation communication systems has been heavily studied. In [1], it has been proposed to use mm-wave frequencies for the 5G to achieve higher data rates. Already in 2017, eleven candidate bands in the frequency range between 24.25 GHz and 86 GHz have been discussed at the World Radiocommunication Conference [2]. To compensate for the path loss at the higher frequencies, high gain phased antenna arrays can be applied [3]. Furthermore, not only the peak gain but also the spatial coverage of the antenna have been recognized as important parameters. Spatial coverage performance is extremely important because the orientation of the mobile device is usually unknown. To characterize the spatial coverage, a metric of coverage efficiency has been introduced in [4] and then applied in [5] to characterize the performance of 5G mm-wave mobile devices.

Multiple mobile phased antenna array solutions already exist in the academic literature. Multi-polarized antenna arrays for the 5G mm-wave were constructed in [6]. A low-profile beam-steerable antenna for 5G mobile terminals was designed and analyzed in [7], and an even smaller antenna array with a clearance of 1.2 mm was proposed in [8]. To increase the 3D coverage of the 5G mobile antenna system, two different methods were proposed in [9] and [10]: folding the antenna structure and surface wave excitation, respectively. By increasing the scan angle, the higher coverage efficiency performance was obtained in [11] and [12]. Circularly polarized antennas for the 5G mobile terminals were developed in [13]–[15], which can improve the BER by always matching the polarization of the antenna and the channel. Then, to steer the beams with low loss and to reduce the system complexity, two passive parasitic elements were applied to scatter the main beam in [16]. Finally, in [17], it has been shown how a 4G MIMO antenna can be integrated with a 5G mm-wave array on the typical ground plane.

However, the user will also have a significant impact on the coverage performance of a mobile phased antenna array. Good coverage with a peak gain of at least 7 dBi is expected from the mobile antenna arrays. However, when the array is subjected to the user effects, the spatial coverage will drop significantly due to the blockage induced by the user, but the body loss is considerably lower than the body loss of sub 5 GHz mobile antennas [18]. However, body blockage at the 28 GHz is not as severe at 60 GHz, which has been investigated in [19]. At the resonant frequency of 15 GHz, the loss due to user effects has been evaluated in [20]. Similar or even greater losses would be expected for the mobile antenna arrays designed at the resonant frequency of 28 GHz, as shown in [18]. Effects of the full metal case and user's hand were also studied in [21], where the gain of at least 6.9 dBi has been achieved even with user effects considered. In [22], the user impact on switch diversity and phased antenna arrays for mobile devices was researched, and it has been found that beamforming is not always advantageous when user effects are considered. However, in the switch diversity case, only a single element on the short edge was studied, but the best array positions on the whole ground plane had not yet been assessed. Finally, in [23], a dual sub-array antenna system for 5G mobile terminals with SAR reduction capabilities was proposed, but it must be noted that in cm-mm-wave bands, power density should be used to evaluate a phantom electromagnetic wave absorption instead of SAR as given in [24]. Switchable phased antenna arrays had already been proposed in [10], but the optimal positions for the antenna array have not yet been found when user effects are considered. In this paper, a method of finding the most suitable locations on the whole ground plane for the 5G mobile terminal phased array is proposed at the frequency of 28 GHz. Then, the antenna array is constructed, based on the proposed guidelines and both measured and simulated

This work was supported by the InnovationsFonden project of RANGE.(Corresponding author: Shuai Zhang).

Igor Syrytsin, Shuai Zhang, and Gert Frølund Pedersen are with the Antennas, Propagation and Millimeter-wave Systems section at the Department of Electronic Systems, Aalborg University, Denmark (email: {igs,sz,gfp}@es.aau.dk).

Art Morris is with wiSpry, Irvine, CA 92618 USA

This article has been accepted for publication in a future issue of this journal, but has not been fully edited. Content may change prior to final publication. Citation information: DOI 10.1109/TAP.2019.2905685, IEEE Transactions on Antennas and Propagation

with the user. In Section II, the optimal positions for a 5G antenna array of four elements in a handset are obtained with the presence of the user effects. Then, in Section III, several planar sub-arrays are placed in the chosen locations on the ground plane. Furthermore, a substrate integrated waveguide (SIW) beamforming lens is applied for each sub-array. Later, the free space measured results of the two sub-arrays with two lenses in one corner are compared to the simulations in the CST Microwave studio. In Section IV, the proposed array is simulated and measured with the user in the talk, data and dual-hand mode, and in Section V, the two common array configurations are investigated. Finally, the effectiveness of the proposed method is assessed in section VI.

II. Optimal Array Position Investigation

In this section, the optimal antenna array positions where the lowest user impact is observed are determined. Here, the array coverage performance losses due to user blockage are the main contributor. The body loss is very low at mm-wave frequencies [18], so it is not an important factor for the investigation. Three setups using the homogeneous phantom as shown in Fig. 1 are considered. The phantom is made of skin tissue with $\varepsilon_r = 19 + 19j$ at 28 GHz. The antenna is simulated in three setups: talk mode in Fig. 1(a), data mode in Fig. 1(b), and dual hand mode in Fig. 1(c). The chosen phantom was first proposed in [25], based on the typical average physical dimensions of a male human being. The left-handed phantom is used in talk and data mode simulations. However, if the right-handed phantom is used, then the radiation patterns will be mirrored along the horizontal axis because of the phantom and antenna array symmetry.

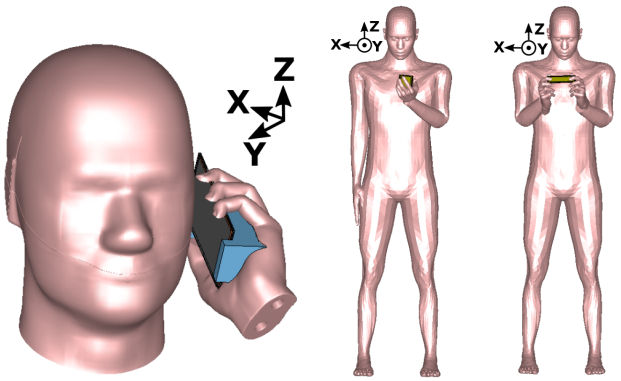

(a) (b) (c)

Fig. 1. Simulation setup with the user in (a) talk mode, (b) data mode, and (c) dual hand mode.

A. Simulation Setup

To investigate the user impact for the different array locations, we considered as many positions as physically possible on a typical ground plane with a size of 63 mm × 132 mm. Furthermore, the performance of the antennas with endfire and broadside radiation was compared at 28 GHz. For the purpose of the study, the antenna structure consisting of 120 antenna elements (64 Vivaldi and 56 slot antenna elements), as shown in Fig. 2, was constructed. The zoomed view of the antenna elements is also demonstrated in Fig. 2. The center-to-center distance between elements is $\lambda/2$ at 28 GHz.

To simplify the investigation, only 4 elements were combined into an array at a time. Each array is a phased array with the maximum scan angle of ±40 degrees. In this study, a sliding array principle was adopted, where each array can be composed of any four neighboring elements, but only linear arrays can be constructed. In Fig. 2, all of the positions of the sliding array are illustrated. A total of 40 Vivaldi (endfire) array positions and 32 of slot (broadside) positions were considered. All antennas were simulated one by one; then, the phased arrays were constructed in post-processing. The phase shifter and feeding network losses have not been accounted for in this work. However, in application these losses will be significant.

The total scan pattern (TSP) and coverage efficiency (CE) were calculated for each position of the sliding arrays. The TSP is extracted from all of the possible radiation patterns produced by the phased array with all the possible phase shifts. At each spatial point, the best possible gain value is chosen. The CE is then calculated from the TSP and describes the spatial coverage of the phased antenna array system. CE is defined as [5]:

$$\eta_c = \frac{\text{Coverage Solid Angle}}{\text{Maximum Solid Angle}} \tag{1}$$

where maximum solid angle is defined as 4π steradians.

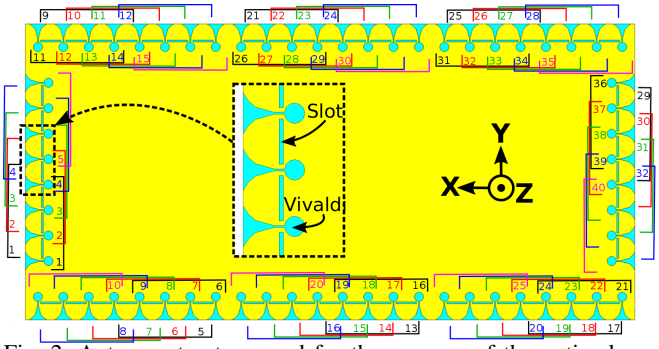

Fig. 2. Antenna structure used for the purpose of the optimal array investigation when user effects are considered. Vivaldi array positions are marked on the inside of the ground plane and the slot array positions are marked on the outside of the ground plane.

B. Best Possible Antenna Performance

In this subsection, the combined endfire array performance is compared to the combined broadside antenna performance. For this purpose, the TSP is calculated for all the possible sliding array positions. The TSP of all possible Vivaldi arrays is shown in Fig. 3. In free space in Fig. 3(a), the endfire arrays cover the region from $\theta = 20°$ to $\theta = 160°$ with high gain of 10 dBi. In contrast, regions where $\theta = 0$ to 20° and $\theta = 160$ to 180° are only covered with a gain of 3 dBi. Next, the TSP for the talk mode is displayed in Fig. 3(b). The shadow from the user's head is visible at $\phi = 300°$ and spans from 40 to 120° in θ, which is much smaller than the shadowing areas measured/simulated in [10], [18], [20], [22]. This already showed that using more sub-arrays distributed around the phone chassis has a beneficial effect on reducing

This article has been accepted for publication in a future issue of this journal, but has not been fully edited. Content may change prior to final publication. Citation information: DOI 10.1109/TAP.2019.2905685, IEEE Transactions on Antennas and Propagation

the user blockage. In Fig. 3(c), the TSP for the data mode is illustrated. The shadowing area at $\phi = 270°$ is also much narrower than the shadowing areas discussed in [10], [18], [20], [22]. Finally, in Fig. 3(d) the shadowing area for dual-hand mode is at least 20° wider in ϕ direction than that observed in the data mode, as shown in in Fig. 3(c). These results are expected because both user's hands are on the mobile device at the same time; thus, more antenna elements are covered.

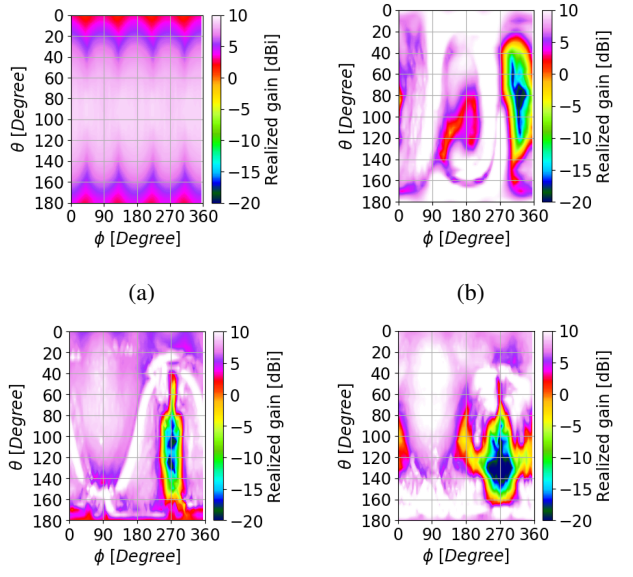

Fig. 3. TSP for all possible sliding Vivaldi arrays in (a) free space, (b) talk mode, (c) data mode, and (d) dual-hand mode.

The TSPs of all possible sliding slot arrays with broadside radiation patterns are shown in Fig. 4. In free space, the slot arrays cover the space opposite to the space of the Vivaldi arrays in Fig. 4(a). However, the gain of slot arrays is lower than the gain of Vivaldi arrays. The shadowing area in total scan patterns of slot arrays is very similar to one of Vivaldi arrays, but the maximum gain in all of the setups with a user is lower. As seen both in Fig. 3 and Fig. 4, the blind spots appear behind the user's body in data and dual-hand modes and behind the head in talk mode. In these blind spots, bad wireless connections at 28 GHz are expected. However, in the indoor scenario, the reflections from the walls, floor and ceiling and diffractions from the corners will contribute to the radiated power in the shadowing region. However, in the outdoor scenario, mostly line of sight components will be dominant, and the number of the scatterers close to the user will be very small.

Next, the CE performance is calculated from the TSPs in Fig. 3 and Fig. 4 and shown in Fig. 5. The CE of the Vivaldi arrays is shown in Fig. 5(a). The 100 % coverage for the threshold gain of 3 dBi can be achieved by these arrays. If the $\eta_c = 0.8$ is considered, the threshold gain in free space is then 7.5 dBi, in talk mode is 0 dBi, in data mode is 6 dBi, and in dual-hand mode is 2.5 dBi. However, in Fig. 5(b), the performance of slot arrays in free space is at least 2 dB

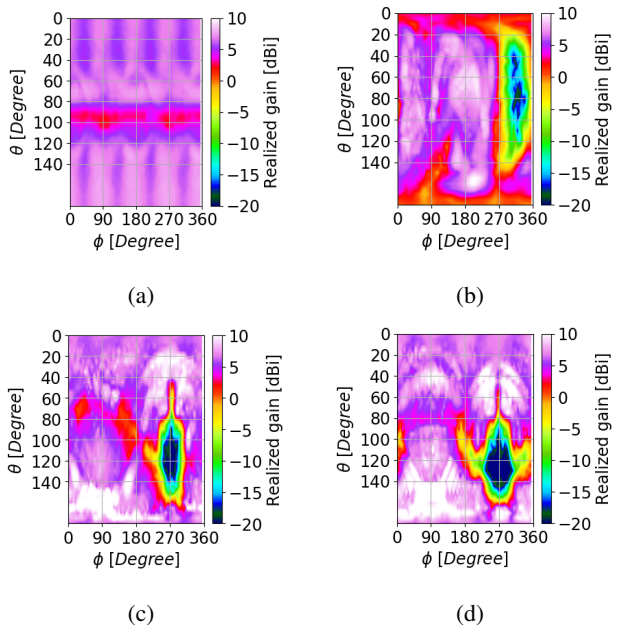

Fig. 4. TSP for all possible sliding slot arrays in (a) free space, (b) talk mode, (c) data mode, and (d) dual-hand mode.

worse for 100 % coverage. At the $\eta_c = 0.8$, the threshold gain of 5 dBi is expected in free space, 0 dBi in talk and dual-hand modes, and 2.5 dBi in data mode. In the region of coverage $\eta_c \leq 0.3$ the threshold gain for the setups with the user is truly higher because the user's body/head becomes an efficient scatterer. From this study, we can conclude that if all the possible sliding array positions are used, then the endfire arrays show better performance both in free space and in user cases.

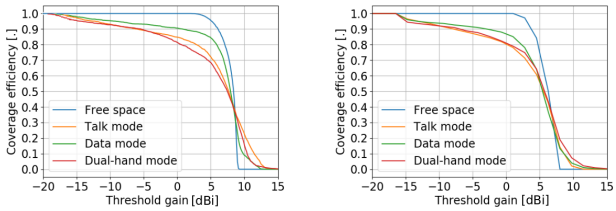

Fig. 5. CE of all possible sliding (a) Vivaldi arrays and (b) slot arrays.

C. Best Position Evaluation

In this subsection, the performance of the sliding 4-element phased array is inspected in each of the positions on the ground plane. The CE is calculated for each sliding array position for both slot and Vivaldi arrays. Hence, four CE curves, like the CE curves displayed in Fig. 5, are obtained for each sliding array position.

To quantify the performance of the sliding array at the specific position, we decided to use metrics of mean threshold gain and coverage efficiency variance (CEV) at the mean threshold gain. These two metrics are calculated at the CE values of $\eta_c = 0.8$, $\eta_c = 0.5$ and $\eta_c = 0.2$. The mean of the threshold gain is calculated from the results in the free space, talk, data, and dual hand modes at the specific coverage efficiency value. The CEV is obtained between the results of talk, data, and dual hand modes at the specific mean gain value

This article has been accepted for publication in a future issue of this journal, but has not been fully edited. Content may change prior to final publication. Citation information: DOI 10.1109/TAP.2019.2905685, IEEE Transactions on Antennas and Propagation

for each curve. The mean gain and variance values are shown for all of the sliding array positions at three specific CE values in Fig. 6.

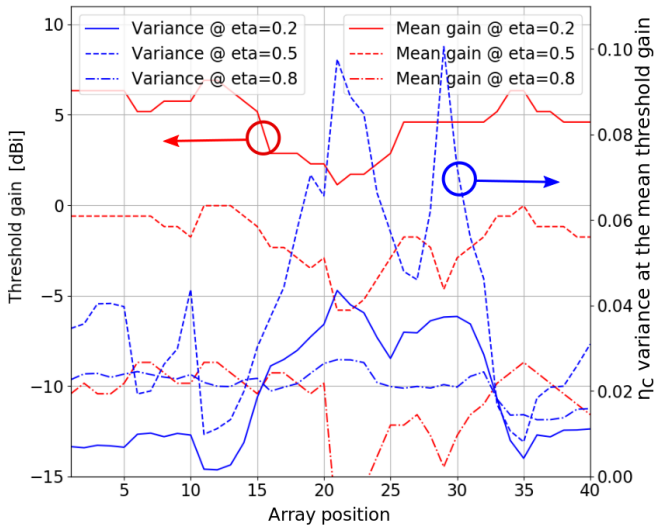

(a)

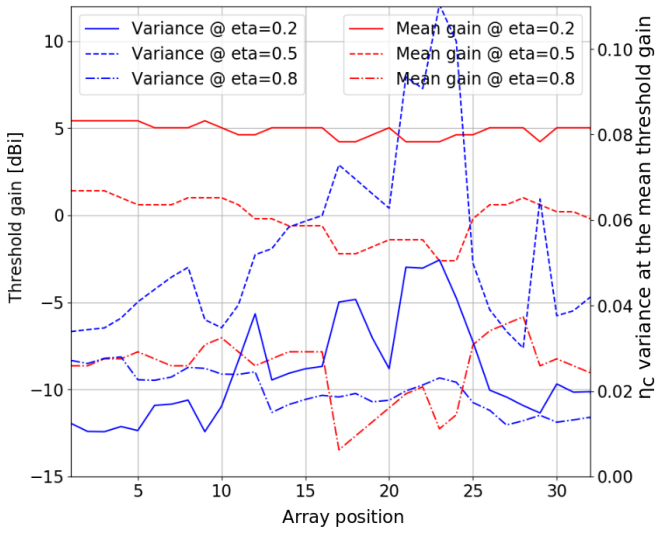

(b)

Fig. 6. Mean threshold gain and CEV between the free space, talk, data and dual-hand modes for (a) Vivaldi arrays, and (b) Slot arrays.

In this investigation, the positions where the mean gain is high and variance is low are considered to be optimal for good array performance because when the variance is low, the difference between the array performance in free space, talk, data, and dual hand modes is smaller. Thus, the antenna is not affected significantly by a user at these positions. In Fig. 6, an interesting trend can be observed. At the positions where the mean gain is high, the variance is low, which ias also true for all chosen values of coverage efficiency $\eta_c = 0.8$, $\eta_c = 0.5$ and $\eta_c = 0.2$. Generally, positions 1 to 15 and positions 35 to 40 are quite good for the endfire (Vivaldi) array placement in Fig. 6(a). Positions 1 to 12 and 25 to 32 are also good for the broadside (slot) array placement in Fig. 6(b).

Next, we investigated how much the mean gain and variance are correlated between the endfire and broadside arrays. The correlation coefficient was calculated between the endfire and broadside arrays in all the positions for all possible coverage efficiency values. The correlations in the mean and variance values are shown in Fig. 7. In all cases, the correlation coefficient is higher than 0.75. In conclusion, the performance of the antenna array does not depend so much on antenna type but mostly on the position of the array on the ground plane.

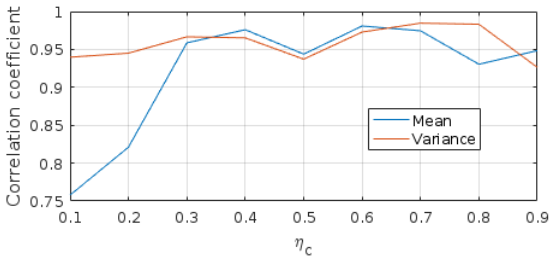

Fig. 7. Correlation coefficient between the broadside and endfire antenna elements.

To illustrate where the best positions of the arrays are located, only the mean gain of the endfire arrays is considered. The endfire array is chosen because it is the array with the most positions on the ground plane. Furthermore, it does not matter which array to choose because of the high correlation between endfire and slot arrays. At $\eta_c = 0.5$, the highest CEV value is observed. The high variance means large performance variation across the data, talk, and dual- hand modes, so the value of $\eta_c = 0.5$ could be considered the worst scenario. The hypothesis is that if the proposed method works for the $\eta_c = 0.5$, then it should work for the other coverage efficiency values as well. The normalized mean gain is shown at $\eta_c = 0.5$ for different positions around the ground plane. The gain alone can be the indicator of a good position because when the gain is high, the variance is low, as shown in Fig. 6. Each position of the 4-element array has been marked by the color of the corresponding normalized mean gain value and is shown in Fig. 8 on a typical mobile phone ground plane. The positions where the mean gain values equal 0 dBi are very suitable for the array placement and represent the best possible gain for the chosen array. At the positions where the color bar value is -3.5 dBi, the mean gain will be at least 3.5 dBi lower than the best possible mean gain with the same coverage. Fig. 8 clearly shows that the best positions are located around the corners of the mobile device. However, if the right-handed phantom is used for the talk and data simulations, then the picture in Fig. 8 will be mirrored along the horizontal axis because of the phantom and antenna array symmetry.

III. Array Implementation With the Lens

Based on the guidelines from Section II, the antenna array was constructed and tested with a real human in the anechoic chamber to verify the effectiveness of the method proposed in Section II. Usually, the phased array prototype is measured element by element and then, the results are combined in post-processing where the beamforming patterns are computed. To

This article has been accepted for publication in a future issue of this journal, but has not been fully edited. Content may change prior to final publication. Citation information: DOI 10.1109/TAP.2019.2905685, IEEE Transactions on Antennas and Propagation

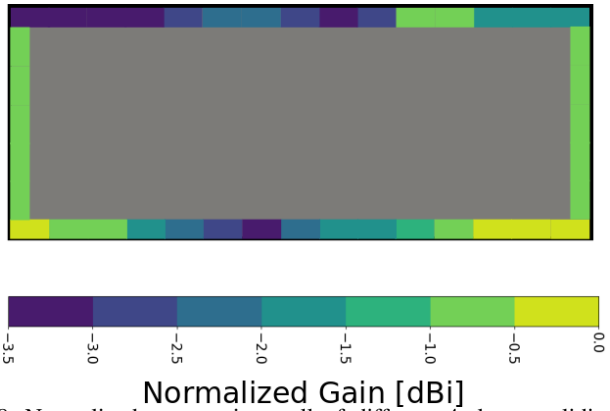

Fig. 8. Normalized mean gain at all of different 4-element sliding array positions around the mobile device ground plane.

obtain the correct beamforming patterns, both the phase and the magnitude of each element should be measured without errors. However, the phase stability is impossible to achieve because fixing a user in a perfect static position during the long measurement is not possible.

Any user will involuntarily make small movements that could be neglected when measuring at the LTE frequencies, but at 28 GHz, even small deviations of 2.5 mm of the antenna position will induce a 90-degree phase error. Applying a full body phantom could be a solution to eliminating the small movements during the measurements. However, at the current time, the full body phantoms at frequencies higher than 3.5 GHz are extremely expensive. Therefore, in this work, the array beamforming is achieved by a lens by switching between the input ports, so no phase shifters or extra post processing steps are required.

In addition, endfire radiation patterns are more preferred in practical applications, which are single directional instead of bi-directional such as broadside radiation patterns. The Vivaldi antenna in Section II has endfire radiation patterns, but the clearance is relatively large. To make the final design more suitable for applications, H-plane horn antennas will be used in the following, which have much smaller clearance and the endfire radiation patterns.

A. Lens Geometry

The four-port SIW lens utilized in this work has a structure similar to the structure described in [26]. However, the angles of SIW and the antenna element type were altered to reduce the total size. The geometry of the SIW lens is shown in Fig. 9. The structure is made on a single layer substrate of Rogers RO3550B with the height of 0.762 mm. Then, four MMPX connectors were used to feed the SIW in Fig. Fig. 9(a). The vias for the lens have a diameter of 1.5 mm, and vias used to feed the SIW have the diameter of 0.4 mm. The distance between vias is 2 mm.

A simple H-plane horn [27] that can be directly excited by SIW is chosen. However, contrary to [27], only two strips are used for the horn to reduce the ground plane clearance. In Fig. 9(b), the ground plane clearance of 2.2 mm has been obtained. The radiating element length is 5.5 mm, and the gap between elements is 0.2 mm.

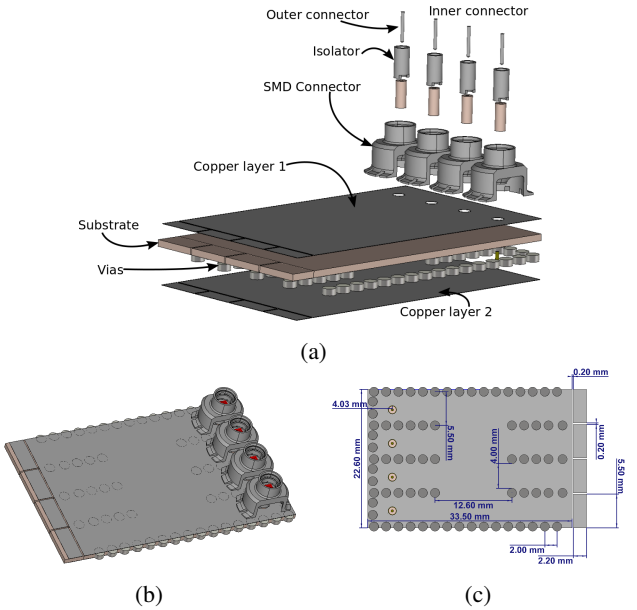

Fig. 9. Antenna array with the lens (a) 3D view and (b) dimensions.

B. Operation Principle

To understand the operating principle of the lens, the maximum surface currents inside the lens are shown in Fig. 10. The purpose of the lens is to convert the TM10 mode of SIW to the TM40 mode inside the lens. Then, TM40 is used to feed the antenna elements at the end of the lens. The lens bends the wave inside the substrate in the clockwise direction when port 1 is excited in Fig. 10(a) and in the counterclockwise direction in Fig. 10(b). The surface current strength on the element 4 in Fig. 10(a) is approximately 4 dB weaker than the surface currents on the other three elements. A similar tendency can be observed for the elements 3 and 4 in Fig. 10(b). As a consequence, the beamwidth of a combined radiation pattern will be slightly larger than ideal. The isolation S32 and S14 are over 10 dB, and the isolation S12 and S34 are higher than 7.7 dB. Furthermore, because of the lens size, the loss in the dielectric is significant at 29.5 GHz. Thus, the efficiency of the proposed lens is -3 dB for ports 2 and 3 and -4 dB for the ports 1 and 4.

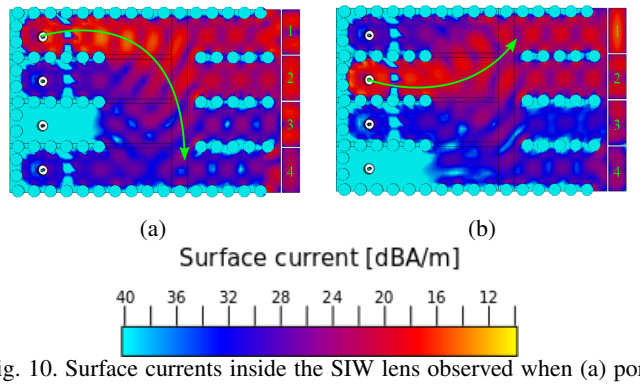

Fig. 10. Surface currents inside the SIW lens observed when (a) port 1 is excited and (b) port 2 is excited.

To investigate how the proposed lens compares to the conventional array of 4 elements, the performance of the array with and without the lens is compared in Fig. 11. In

This article has been accepted for publication in a future issue of this journal, but has not been fully edited. Content may change prior to final publication. Citation information: DOI 10.1109/TAP.2019.2905685, IEEE Transactions on Antennas and Propagation

the array without a lens, the antenna elements are excited directly by the waveguide ports. The phase shift steps used for the beamforming setup are (-100, -50, 50, 100 degrees), which means that the maximum phase shift needed for the four-element array is ±300°. The performance of the phased array is comparable to the implementation with the lens in Fig. 11, but the sidelobes are higher for the lens. Nonetheless, to implement this 4-element phased array, a maximum phase shift of ±300° is required. In the application, phase shifters with such requirements will make the array more lossy than the lens, which only requires a switch.

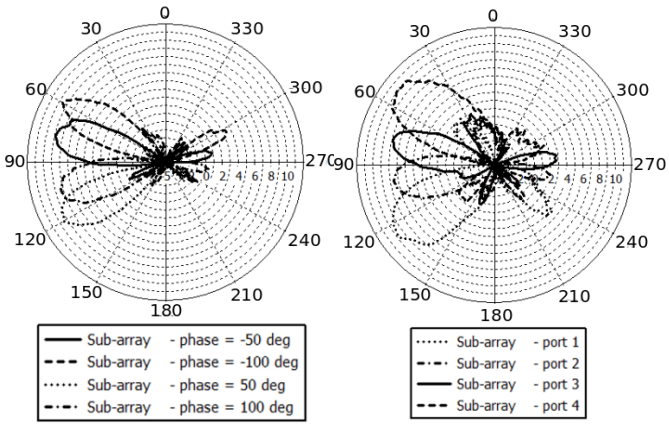

(a) (b)

Fig. 11. Performance comparison of (a) phased array implementation and (b) lens implementation.

C. lens Integration

In this subsection, the lens proposed in Subsection III-A is integrated on a big ground plane. The ground plane size corresponds to the size of a typical mobile device and is shown in Fig. 12(a). The two sub-arrays are placed on the corner of the ground plane. Three layers of copper with 2 layers of the substrate are used in the design in Fig. 12(a). Furthermore, to reduce the ground plane influence on the antenna elements, the small reflectors with the height of 3 mm are added on each side of the ground plane.

The reflection coefficients for both sub-arrays are shown in Fig. 13. Reflection coefficients of the measured lens are generally shifted towards lower frequencies. Furthermore, for ports 1 and 4, two resonances are obtained from the measurements, but only one is obtained in the simulations in Fig. 13(a) and Fig. 13(b). The two lenses are identical, but because connectors have not been mounted perfectly, the difference in matching between the lenses can be observed. Notice here that the lens is operating optimally at the frequency of 29.5 GHz. This frequency is different from the one used for investigation in Section II. However, the difference in the user impact at 28 and 29.5 GHz is insignificant.

Next, the proposed dual sub-array system is measured in the anechoic chamber as shown in Fig. 12(b). In this investigation, we propose to use the antenna system with two sub-arrays on each corner, according to the suggestions from Section II. However, to simplify the manufacturing process, we chose

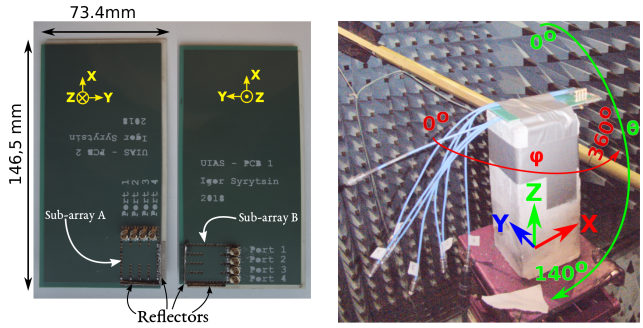

(a) (b)

Fig. 12. (a) two prototype PCBs with one sub-array on each and (b) prototype measured in the anechoic chamber.

to make a prototype with only two sub-arrays. However, in the investigation, the ground plane is rotated around the X-axis and Y-axis to obtain radiation patterns in all the desired directions, as shown in Fig. 14.

The calculated TSP from the simulations and the measurements of the total combined system of 8 sub-arrays are shown in Fig. 15. The directions of the radiation for each sub-array are similar. In the simulations, the radiation patterns obtained by exciting ports 1 and 4 of each SIW lens have a higher maximum gain than the radiation patterns obtained by exciting ports 2 and 3. However, in the measurements, the radiation patterns of ports 2 and 3 have the highest maximum gain. Finally, the CE of the proposed system is calculated and shown in Fig. 18. The CE curve for the measurements is steeper.

IV. User Impact

First, in Section II, we proposed to put antenna arrays in the corners of the mobile phone ground plane. To account for the left-handed and right-handed users, we chose to place a lens in all the corners of the ground plane, as shown in Fig. 14. To verify the proposal of Section II, the prototype was simulated and measured in free space, talk, data, and dual-hand modes, as shown in Fig. 1. In measurements, the phantom is replaced by a user with dimensions like a phantom, as shown in Fig. 16. The same user was participating in the measurements and in the phantom accuracy verification in [25]. The rope has been used in all three setups to secure the user. The foam stand is added to the measurement setup to ensure that the height, angle, and distance to the body remain constant and similar to the simulations.

The radiation patterns at each lens port are measured, and the prototype is rotated to replicate the similar setup, as described in Fig. 14. A TSP is calculated for each of the setups and is shown in Fig. 17. In the talk mode depicted in Fig. 17(a), the shadow from the head appears bigger than the shadow from the head in the measurement in Fig. 17(b). In Fig. 17(c), the shadow looks similar to the measurement of the prototype in the data mode in Fig. 17(d). However, the power behind the user is stronger in the measurement of data mode. Similar conclusions can be drawn from the comparison between simulated and measured results for the dual-hand mode in Fig. 17(e) and Fig. 17(f). However, the shadowing from the head is smaller in the simulations. In all

This article has been accepted for publication in a future issue of this journal, but has not been fully edited. Content may change prior to final publication. Citation information: DOI 10.1109/TAP.2019.2905685, IEEE Transactions on Antennas and Propagation

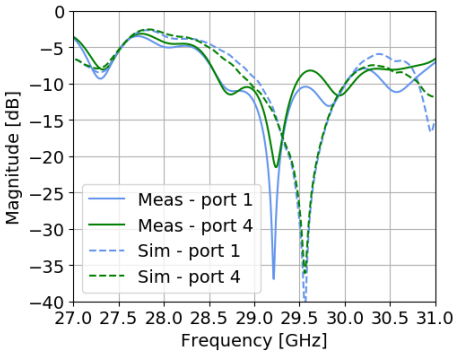

(a)

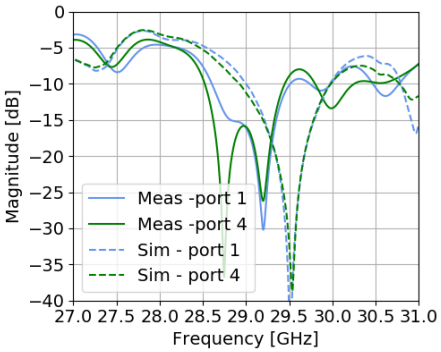

(b)

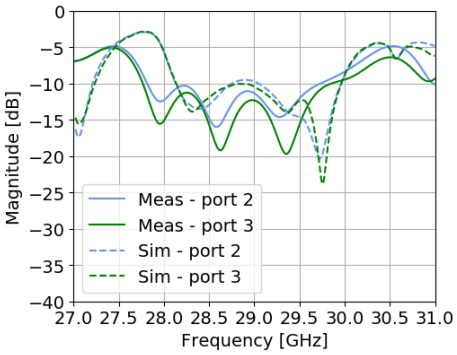

(c)

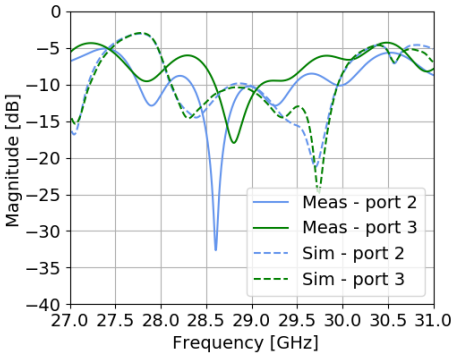

(d)

Fig. 13. Reflection coefficients of the (a) Sub-array A at ports 1 and 4, (b) Sub-array B at ports 1 and 4, (c) Sub-array A at ports 2 and 3, and (d) Sub-array B at ports 2 and 3.

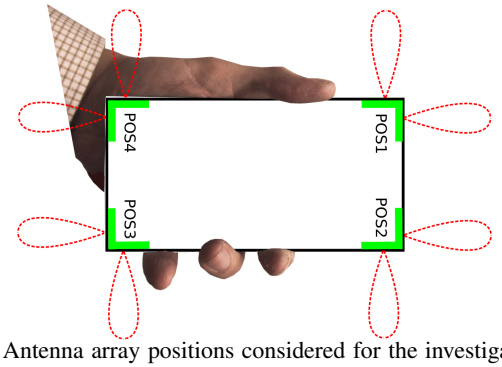

Fig. 14. Antenna array positions considered for the investigation and corresponding radiation pattern directions. The hand has been added to illustrate the grip example with the left hand.

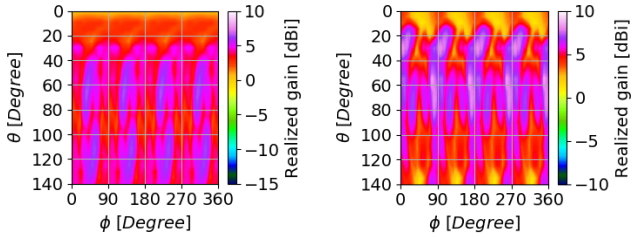

(a) (b)

Fig. 15. Total scan pattern of the (a) simulated and (b) measured SIW lens antenna system.

the measurements, the user appears to be able to redirect a considerable amount into the shadow.

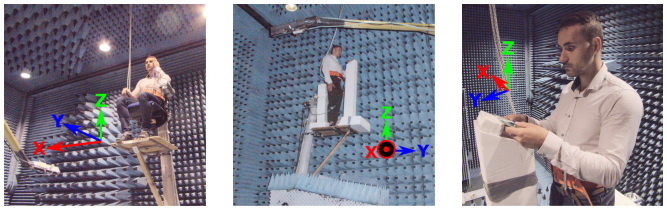

(a) (b) (c)

Fig. 16. Measurement setups with the user in (a) talk mode, (b) data mode, and (c) dual-hand mode.

Finally, the coverage performance results from the measurements and simulations are compared for the four setups in Fig. 18. First, the spread between the data mode, talk mode, and free space curves is larger in the measurements. For the CE of 0.5, the value of threshold gain of 2.5 dBi can be observed in simulations for data and dual-hand modes and 3 dBi for the talk mode in Fig. 18(a). However, in measurements, the gain value of 2.5 dBi at $\eta_c = 0.5$ is obtained in dual-hand mode. Then, the gain of 1.5 dBi and 0.5 dBi is achieved for the data and talk modes, respectively. The performance of the prototype in talk mode is quite different from simulations to measurements, which can be explained by the grip of the user. In talk mode, the user's grip is a very important parameter for the antenna performance, but it is very difficult to replicate the simulated CTIA grip with the actual user.

In [25], a loss of 8.5 dB from free space to talk and data mode curves at $\eta_c = 0.5$ is observed. In [20], a loss of 7.5 to 10 dB is observed for the talk mode, and a loss of approximately 3 dB is observed for the data mode. However, the results in [20] cannot be directly compared to the design proposed in this

This article has been accepted for publication in a future issue of this journal, but has not been fully edited. Content may change prior to final publication. Citation information: DOI 10.1109/TAP.2019.2905685, IEEE Transactions on Antennas and Propagation

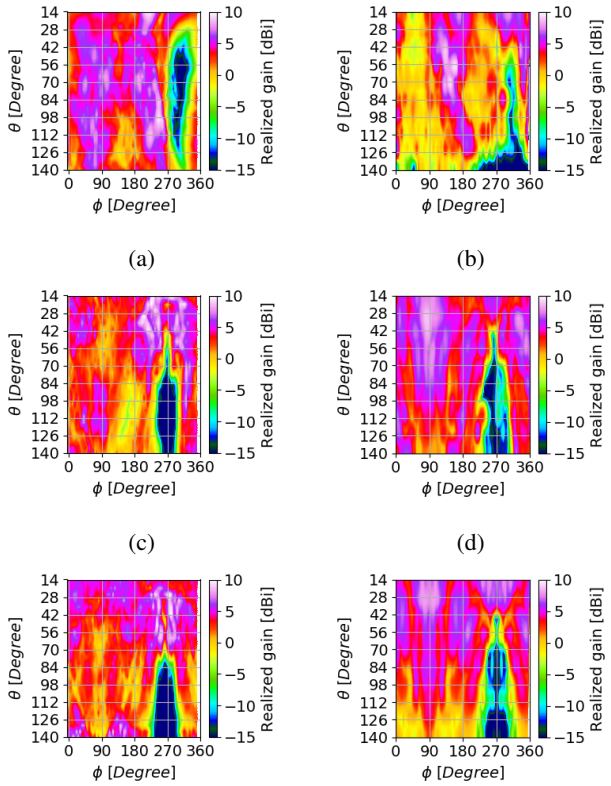

Fig. 17. Total scan patterns of the user (a) simulated in talk mode, (b) measured in talk mode, (c) simulated in data mode, (d) measured in data mode, (e) simulated in dual-hand mode, and (f) measured in dual-hand mode.

paper, because the frequency in [20] is 12 GHz lower; thus, an actual user will affect the waves differently. In this work, a loss of 2.5 dB for the dual-hand mode, 3 dB for the data mode, and 4.5 dB for the talk mode is observed for $\eta_c = 0.5$. These values are lower than the loss observed in the previous works. Furthermore, the talk mode could be considered not as important because an actual user will usually use GSM in talk mode and the fast data rate 5G mm-wave in data and dual-hands modes.

V. Investigation of Other Array Configurations

Next, we chose to investigate how the popular [28] alternative array configurations will affect the coverage performance. We investigated how the performance of the sub-array arrangement in positions 1 and 3 (configuration A) compares to the performance of sub-array arrangement in positions 2 and 4 (configuration B), as shown in Fig. 14. Here, we show only the measured results because they represent the actual scenario.

The TSP for free space, talk, data, and dual-hand modes is depicted in Fig. 19. The free space TSPs for both configurations will be the same but shifted by 90° in ϕ direction, which we have chosen not to show here, as user effects are the main purpose of this investigation. However, in the talk mode, the position of the shadow is different because of the different antenna positions with respect to the user's head, as shown in Fig. 19(a) and Fig. 19(b). An interesting observation can be made for results in a data mode in Fig. 19(d), where

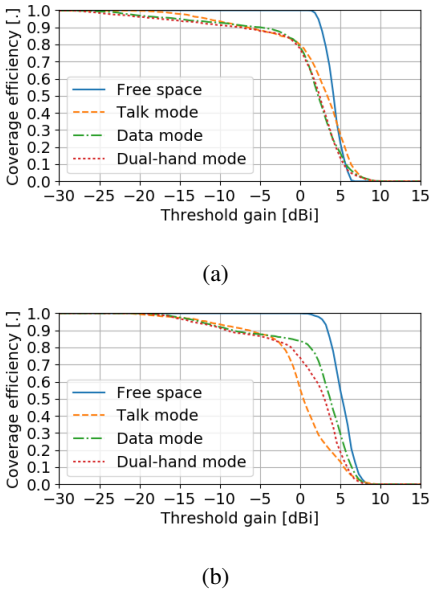

Fig. 18. Coverage efficiency of the (a) simulated and (b) measured antenna system.

the power inside the shadowing area is much stronger than the power inside the shadowing area in Fig. 19(c). We speculate that the antenna array proximity to the skin in configuration B will excite a surface wave on the user's hand and thus transfer more power behind the user. Finally, in the dual-hand mode in Fig. 19(e) and Fig. 19(f), the TSPs look very similar, as expected from the setup symmetry.

Next, the CE is calculated for both configurations and shown in Fig. 20. Instantly, we notice that configuration A is the best to use in the data mode. At a CE level of 0.5, the value of the threshold gain of -2 dBi is observed for configuration B and 2.5 dBi for configuration A, which yields an improvement of 4.5 dB. The CE curves for dual-hand mode are very similar, as expected from the setup symmetry. Finally, only a very small improvement in talk mode only could be seen for the high coverage region ≤ 0.7, where the configuration B is better. However, we can conclude that to account for both right- and left-handed users, the final setup used in the applications should include arrays in all four corners of the device, as shown in Fig. 14.

VI. Assessment of Method's Effectiveness

In this section, the effectiveness of the method that helps to find the best possible position for the array discussed in Section II will be verified. First, to make a fair comparison, the elements in Fig. 2 are arranged into the same configuration as shown in Fig. 14, as has been demonstrated to be advantageous in Section V. In Section II, it has already been established that the user effects on the antenna depend strongly on the antenna locations and not the antenna type. Thus, we chose to consider only endfire (Vivaldi) arrays from Section II.

To verify if the method proposed in Section II works, the mean and variance of the coverage efficiency have been computed for all possible sliding Vivaldi array positions corresponding to Fig. 5(a). If the method proposed in this paper is valid, then both CE mean and variance should be similar for

This article has been accepted for publication in a future issue of this journal, but has not been fully edited. Content may change prior to final publication. Citation information: DOI 10.1109/TAP.2019.2905685, IEEE Transactions on Antennas and Propagation

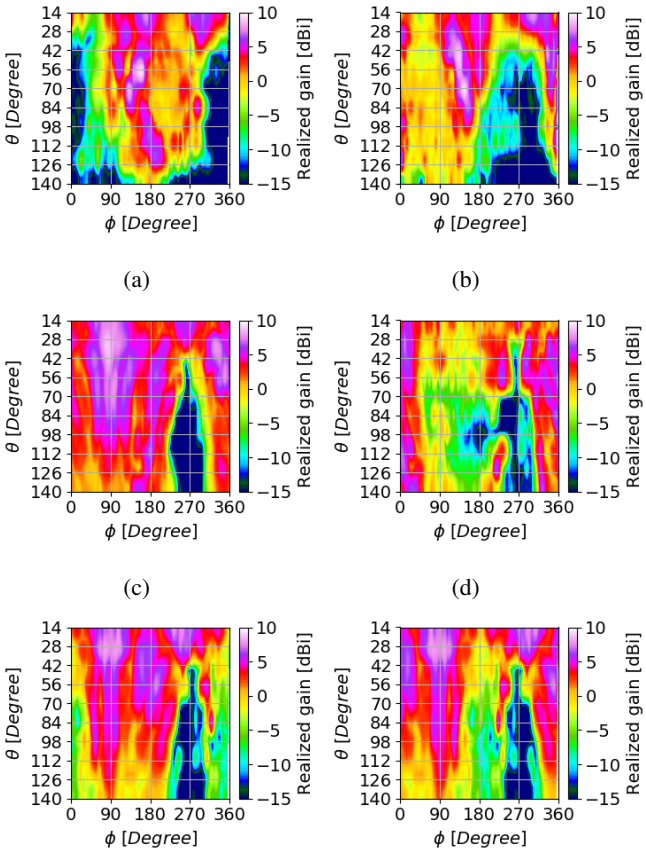

Fig. 19. Measured total scan patterns of the user (a) conf. A – free space, (b) conf. – free space, (c) conf. A – talk mode, (d) conf. B – talk mode, (e) conf. A – data mode, (f) conf. B – data mode, (g) conf. A – dual-hand mode, and (h) conf. B – dual-hand mode.

the case with the sliding Vivaldi array (best possible scenario) and the corner Vivaldi array in the configuration, as presented in Fig. 14. As seen here, both CE mean and variance are indeed similar for these two cases as shown in Fig. 21.

Finally, the Vivaldi antenna arrays are compared to the SIW lens arrays in a similar way. Notice that the loss of the lens is on average approximately 4 dB, which does not occur in the Vivaldi arrays, so the curves for the Vivaldi arrays are moved 4 dB to the right to obtain the fair comparison, as shown in Fig. 21. All the mean coverage efficiency curves have a very similar shape, but the curves for the variance in Fig. 21(b) have a slight difference, especially at the part with the peak variance. Endfire arrays have 2 dB lower peak variance than the results of the simulated SIW lens system. Additionally, the measured SIW lens system has 5 dB higher maximum variance than the endfire arrays. However, the measured results show lower variance for the threshold gain below -10 dBi. From this assessment, we can conclude that the method proposed in Section II, as expected, can be used for determining the best location for any antenna type, as the user impact depends strongly on the antenna location instead of the antenna type.

VII. Conclusion

In this paper, the guidelines for the best possible positions of the 4-element phased 5G mobile array are presented. In

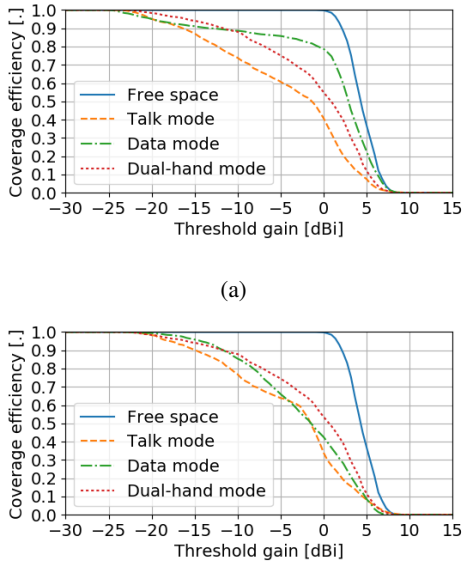

Fig. 20. Total scan pattern of the sub-arrays arranged in (a) configuration A and (b) configuration B.

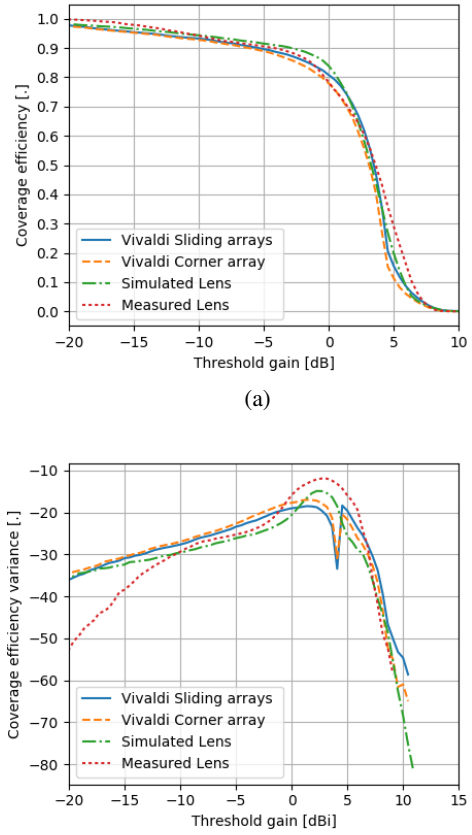

Fig. 21. Comparison of the sliding arrays, corner arrays, measured and simulated lenses by computing (a) mean coverage efficiency and (b) coverage efficiency variance.

this paper, simulations and measurements were performed in three different user-antenna setups: data mode, talk mode and dual-hand mode. The user shadowing effects can be efficiently suppressed with arrays in all four corners of the mobile phone chassis. Then, based on these guidelines, the antenna array was constructed and tested with the real humans in the anechoic chamber to verify the effectiveness of the guidelines. To obtain the correct beamforming patterns with the user and avoid phase errors, the SIW lens sub-array implementation was chosen. The proposed setup is compared to the one with the Vivaldi arrays in two different configurations. A very small difference in the mean and variance of coverage efficiency was found. Thus, the proposed guidelines in this paper are general and can be used for any 5G mm-wave antenna type.

REFERENCES

[1] T. S. Rappaport, S. Sun, R. Mayzus, H. Zhao, Y. Azar, K. Wang, G. N. Wong, J. K. Schulz, M. Samimi, and F. Gutierrez, "Millimeter wave mobile communications for 5G cellular: It will work!," *IEEE Access*, vol. 1, pp. 335–349, 2013.

[2] J. Lee, E. Tejedor, K. Ranta-aho, H. Wang, K. T. Lee, E. Semaan, E. Mohyeldin, J. Song, C. Bergljung, and S. Jung, "Spectrum for 5G: Global status, challenges, and enabling technologies," *IEEE Comm. Mag.*, vol. 56, pp. 12–18, Mar. 2018.

[3] W. Roh, J. Y. Seol, J. Park, B. Lee, J. Lee, Y. Kim, J. Cho, K. Cheun, and F. Aryanfar, "Millimeter-wave beamforming as an enabling technology for 5G cellular communications: theoretical feasibility and prototype results," *IEEE Commun. Mag.*, vol. 52, pp. 106–113, February 2014.

[4] M. U. Rehman, X. Chen, C. G. Parini, and Z. Ying, "Evaluation of a statistical model for the characterization of multipath affecting mobile terminal GPS antennas in sub-urban areas," *IEEE Trans. Antennas Propag.*, vol. 60, pp. 1084–1094, Feb. 2012.

[5] J. Helander, K. Zhao, Z. Ying, and D. Sjöberg, "Performance analysis of millimeter-wave phased array antennas in cellular handsets," *IEEE Antenna Wireless Propag. Lett.*, vol. 15, pp. 504–507, 2016.

[6] W. Hong, S. T. Ko, Y. Lee, and K. H. Baek, "Multi-polarized antenna array configuration for mmwave 5G mobile terminals," *2015 International Workshop on Antenna Technology (iWAT)*, pp. 60–61, Mar. 2015.

[7] W. Hong, K. Baek, Y. Lee, and Y. G. Kim, "Design and analysis of a low-profile 28 GHz beam steering antenna solution for future 5G cellular applications," *Microwave Symposium (IMS), 2014 IEEE MTT-S International*, pp. 1–4, Jun. 2014.

[8] I. Syrytsin, S. Zhang, G. F. Pedersen, and A. Morris, "Compact quad-mode planar phased array with wideband for 5G mobile terminals," *IEEE Trans. Antennas Propag.*, 2018,(in press).

[9] N. Ojaroudiparchin, M. Shen, S. Zhang, and G. F. Pedersen, "A switchable 3-D-coverage-phased array antenna package for 5G mobile terminals," *IEEE Antennas Wireless Propag. Lett.*, vol. 15, pp. 1747–1750, 2016.

[10] S. Zhang, X. Chen, I. Syrytsin, and G. F. Pedersen, "A planar switchable 3-D-coverage phased array antenna and its user effects for 28-GHz mobile terminal applications," *IEEE Trans. Antennas Propag.*, vol. 65, pp. 6413–6421, Dec 2017.

[11] N. Ojaroudiparchin, M. Shen, and G. F. Pedersen, "Wide-scan phased array antenna fed by coax-to-microstriplines for 5G cell phones," *2016 21st International Conference on Microwave, Radar and Wireless Communications (MIKON)*, pp. 1–4, 2016.

[12] N. O. Parchin, M. Shen, and G. F. Pedersen, "End-fire phased array 5G antenna design using leaf-shaped bow-tie elements for 28/38 GHz MIMO applications," *2016 IEEE International Conference on Ubiquitous Wireless Broadband (ICUWB)*, pp. 1–4, 2016.

[13] K. R. Mahmoud and A. M. Montaser, "Design of dual-band circularly polarised array antenna package for 5g mobile terminals with beam-steering capabilities," *IET Microwaves, Antennas Propagation*, vol. 12, no. 1, pp. 29–39, 2018.

[14] I. Syrytsin, S. Zhang, and G. F. Pedersen, "Circularly polarized planar helix phased antenna array for 5G mobile terminals," in *2017 International Conference on Electromagnetics in Advanced Applications (ICEAA)*, pp. 1105–1108, Sept 2017.

[15] S. Zhang, I. Syrytsin, and G. F. Pedersen, "Substrate-insensitive phased array with improved circularly-polarized scan angle for 5G mobile terminals," in *2017 12th European Conference on Antennas and Propagation (EUCAP)*, Apr. 2018.

[16] S. Zhang, I. Syrytsin, and G. F. Pedersen, "Compact beam-steerable antenna array with two passive parasitic elements for 5G mobile terminals at 28 GHz," *IEEE Trans. Antennas Propag.*, 2018,(in press).

[17] R. Hussain, A. T. Alreshaid, S. K. Podilchak, and M. S. Sharawi, "Compact 4G MIMO antenna integrated with a 5G array for current and future mobile handsets," *IET Microwaves, Antennas & Propagation*, vol. 11, no. 2, pp. 271–279, 2017.

[18] I. Syrytsin, S. Zhang, G. F. Pedersen, K. Zhao, T. Bolin, and Z. Ying, "Statistical investigation of the user effects on mobile terminal antennas for 5G applications," *IEEE Trans. Antennas Propag.*, vol. 65, pp. 6596–6605, Dec 2017.

[19] T. Wang, M. Umehira, H. Otsu, S. Takeda, T. Miyajima, and K. Kagoshima, "A twin cylinder model for moving human body shadowing in 60GHz wlan," in *2015 21st Asia-Pacific Conference on Communications (APCC)*, pp. 188–192, Oct 2015.

[20] K. Zhao, J. Helander, D. Sjöberg, S. He, T. Bolin, and Z. Ying, "User body effect on phased array in user equipment for the 5G mmwave communication system," *IEEE Antenna Wireless Propag. Lett.*, vol. 16, pp. 1847–1850, 2017.

[21] B. Yu, K. Yang, C. Y. D. Sim, and G. Yang, "A novel 28 GHz beam steering array for 5G mobile device with metallic casing application," *IEEE Trans. Antennas Propag.*, vol. 66, pp. 462–466, Jan. 2018.

[22] I. Syrytsin, S. Zhang, and G. F. Pedersen, "User impact on phased and switch diversity arrays in 5G mobile terminals," *IEEE Access*, vol. 6, pp. 1616–1623, 2018.

[23] J. Bang and J. Choi, "A SAR reduced mm-wave beam-steerable array antenna with dual-mode operation for fully metal-covered 5G cellular handsets," *IEEE Antenna Wireless Propag. Lett.*, vol. 17, pp. 1118–1122, Jun. 2018.

[24] B. Xu, K. Zhao, B. Thors, D. Colombi, O. Lundberg, Z. Ying, and S. He, "Power density measurements at 15 GHz for RF EMF compliance assessments of 5G user equipment," *IEEE Trans. Antennas Propag.*, vol. 65, pp. 6584–6595, Dec 2017.

[25] I. Syrytsin, S. Zhang, G. F. Pedersen, and Z. Ying, "User effects on the circular polarization of 5G mobile terminal antennas," *IEEE Trans. Antennas Propag.*, vol. 66, pp. 4906–4911, Sep. 2018.

[26] Y. J. Cheng and Y. Fan, "Millimeter-wave miniaturized substrate integrated multibeam antenna," *IEEE Trans. Antennas Propag.*, vol. 59, pp. 4840–4844, Dec 2011.

[27] L. Wang, M. Garcia-Vigueras, M. Alvarez-Folgueiras, and J. R. Mosig, "Wideband H-plane dielectric horn antenna," *IET Microwaves, Antennas Propagation*, vol. 11, no. 12, pp. 1695–1701, 2017.

[28] W. Hong, K. H. Baek, and S. Ko, "Millimeter-wave 5G antennas for smartphones: Overview and experimental demonstration," *IEEE Trans. Antennas Propag.*, vol. 65, pp. 6250–6261, Dec 2017.

Igor Syrytsin was born in Saratov, Russia, in 1988. He received the B.S. degree in electronic engineering and IT and M.S. degree in wireless communication systems from Aalborg University, Aalborg, Denmark, in 2014 and 2016, respectively. Currently, he is pursuing the Ph.D. degree at Department of Electronic Systems at Aalborg University. His research interests include mm-wave mobile antenna design and interactions between user and mobile antennas.

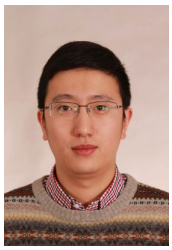

Shaui Zhang received the B.E. degree from the University of Electronic Science and Technology of China, Chengdu, China, in 2007 and the Ph.D. degree in electromagnetic engineering from the Royal Institute of Technology (KTH), Stockholm, Sweden, in 2013. After his Ph.D. studies, he was a Research Fellow at KTH. In April 2014, he joined Aalborg University, Denmark, where he currently works as Associate Professor. In 2010 and 2011, he was a Visiting Researcher at Lund University, Sweden and at Sony Mobile Communications AB, Sweden, respectively. He was also an external antenna specialist at Bang & Olufsen, Denmark from 2016-2017. He has coauthored over 40 articles in well-reputed international journals and over 14 (US or WO) patents. His research interests include: mobile terminal mm-wave antennas, biological effects, CubeSat antennas, UWB wind turbine blade deflection sensing, MIMO antenna systems, and RFID antennas.

Gert Frølund Pedersen was born in 1965. He received the B.Sc. and E.E. (Hons.) degrees in electrical engineering from the College of Technology in Dublin, Dublin Institute of Technology, Dublin, Ireland, in 1991, and the M.Sc.E.E. and Ph.D. degrees from Aalborg University, Aalborg, Denmark, in 1993 and 2003, respectively. Since 1993, he has been with Aalborg University where he is a Full Professor heading the Antenna, Propagation and Networking LAB with 36 researchers. He is also the Head of the Doctoral School on wireless communication with some 100 Ph.D. students enrolled. His research interests include radio communication for mobile terminals especially small antennas, diversity systems, propagation, and biological effects. He has published more than 175 peer reviewed papers and holds 28 patents. He has also worked as a Consultant for developments of more than 100 antennas for mobile terminals including the first internal antenna for mobile phones in 1994 with lowest SAR, first internal triple-band antenna in 1998 with low SAR and high TRP and TIS, and lately various multiantenna systems rated as the most efficient on the market. He has worked most of the time with joint university and industry projects and have received more than 12 M$ in direct research funding. He is currently the Project Leader of the SAFE project with a total budget of 8 M$ investigating tunable front end including tunable antennas for the future multiband mobile phones. He has been one of the pioneers in establishing over-the-air measurement systems. The measurement technique is now well established for mobile terminals with single antennas and he was chairing the various COST groups (swg2.2 of COST 259, 273, 2100, and now ICT1004) with liaison to 3GPP for over-the-air test of MIMO terminals. He is currently involved in MIMO OTA measurement.

Arthur S. Morris III (S'90–M'91–SM'04–F'13) received the B.S. degree in physics and also in electrical engineering and M.S. and Ph.D. degrees in electrical engineering from North Carolina State University (NCSU), Raleigh, NC, USA, in 1983, 1986, and 1993, respectively. As a Scientist/Engineer with a concentration on physical electronics and electromagnetic fields for over 30 years, he has contributed to device technologies ranging from traveling-wave tubes to millimeter-wave heterojunction bipolar transistors and has developed products for markets from high-voltage instrumentation to broadband communication systems. In 1999, he joined Coventor, to lead software and hardware development to drive the transition of microelectromechanical systems (MEMS) and microsystems from the laboratory into products for RF and optical applications. He is a cofounder of Wispry Inc., Irvine, CA, USA, which spun out of Coventor in 2002. He is the company's Chief Technical Officer (CTO) and leads the development of high-performance programmable RF products for high-volume markets utilizing MEMS, CMOS, and advanced packaging. He is an Adjunct Professor with NCSU.